ELSEVIER

Physica D 152–153 (2001) 288–309

PHYSICA D

www.elsevier.com/locate/physd

Methods for the exact construction of mesoscale spatial structures in liquid crystal polymers☆

M. Gregory Forest[a,*], Qi Wang[b], Hong Zhou[c]

[a] *Department of Mathematics, University of North Carolina, CB 3250, Phillips Hall, Chapel Hill, NC 27599-3250, USA*
[b] *Department of Mathematical Sciences, Indiana University-Purdue University Indianapolis, Indianapolis, IN 46202, USA*
[c] *Department of Mathematics, University of California, Santa Cruz, CA 95064, USA*

Abstract

We examine orientational patterns of liquid crystalline polymers (LCPs) using a mesoscale Doi theory that couples short-range, excluded-volume molecular interactions, rotary molecular diffusion, and the Marrucci–Greco potential for finite-range distortional elasticity. The model is a full tensor, polymeric generalization of small-molecule liquid crystal (Ericksen–Leslie) theory. The symmetric, traceless, rank 2 orientation tensor corresponds to micron-scale, averaged 3D microstructure through an orthogonal frame of eigenvectors (the directors, or principal optical axes) and corresponding eigenvalues (the order parameters) which convey the degrees of orientation with respect to the optical axes. These model quantities are directly related to intensity data from light scattering experiments. We focus on a classical method, separation of variables, to provide an exact construction of spatial patterns, both steady and time-dependent. Our constructions arise from posited tensor representations in spectral variables, separating spatial structure arising from optical axes variations versus order parameter variations. The reduced equations are solved to generate a variety of mesoscale structures, presented both in terms of the geometric content of the orientation tensor and in terms of the light scattering intensity patterns which would result from these exact macromolecular structures.

Keywords: Liquid crystalline polymers; Mesoscale Doi tensor theory; Spatial structures

1. Introduction

Experimental observations [4,7,15] of liquid crystal polymers (LCPs), either in weak flows such as simple shear or subsequent to cessation of an imposed shear or elongation, exhibit distinct and reproducible patterns. Examples of such structures are banded or striped patterns, which are widely accepted as being the result of mesoscale optical axes which vary sinuously along a particular direction selected by the experiment. There are computational studies, e.g., those of Tsuji and Rey [22], which exhibit banded patterns. Our motivation is an understanding of the origin of these and other distinguished mesoscale structures. We surmise that many heterogeneous spatial patterns are natural states of the material that exist in the competition between various competing nematic macromolecular

☆ This paper is dedicated to Prof. Zakharov, and his remarkable and unparalleled intuition for inherent mathematical order in complex nonlinear physical systems. From the first reading of the 1972 soliton gem by Zakharov and Shabat [25], to the modern exact solutions of weak turbulence theory [23,24], the power of imagination roaming between mathematics and physical systems remains an inspiration for all ages.

* Corresponding author.
E-mail address: forest@amath.unc.edu (M.G. Forest).

0167-2789/01/$ – see front matter
PII: S0167-2789(01)00175-0

potentials (e.g., short-range excluded volume and intermediate-range distortional elasticity). Certain experimental conditions, such as an imposed shear or elongation, are required to access and select these states versus an alternative explanation that the experiment creates the patterns. Our scenario is plausible especially in light of the fact that the patterns persist for decades of elastic relaxation timescales of the LCP. Given this picture, we therefore explore analytical constructions of families of basic patterns from accepted continuum models of LCPs. The solution families should be general enough (i.e. possessing continuous degrees of freedom) for an experiment to yield a selection mechanism.

To seek analytical constructions of patterns, we have to choose from the various continuum models relevant to the experimental lengthscales at which the patterns are observed. Sophisticated theories for materials with anisotropic microstructure have been developed and applied to various dynamical problems, in which orientation dynamics is coupled with hydrodynamics [2,3,14]. For flows of liquid crystalline polymers, the Doi theory for homogeneous LCPs has been tested extensively in various simple as well as complex flow geometries [8,9,15,16]. The Doi–Edwards theories [6] begin with a homogeneous excluded-volume potential, following the classical results of Maier–Saupe [17] and Onsager [20]. This potential resolves the isotropic-to-nematic (I–N) phase transition as opposed to Leslie–Ericksen theory which assumes the nematic state at the outset and does not resolve the I–N transition. This element of the Doi-type theories alone compels one to dispel the seminal, though limited, single director theories. To account for the heterogeneity in these materials, Marrucci and Greco introduced a nonlocal term describing the elastic distortional coupling among neighboring molecules, which is the tensorial analog of Frank elasticity in Leslie–Ericksen models. The Doi theory with the Marrucci–Greco potential, referred to as the Doi–Marrucci–Greco (DMG) theory, is the basis of many current approaches to capture intricate LCP temporal–spatial structures, with and without flows (see, [1,2,4,6,8–13,15,16,18,22] and others cited therein).

The goal of this paper is to analyze systematically those *spatial structures supported by the DMG model purely from material effects*. Thus, we focus here on structures that are supported by the interplay between short-range excluded-volume effects and an elastic distortional potential. We develop a simple separation of variables technique applied to the spectral representation of the orientation tensor.

Molecular orientation and fluid flow are 3D phenomena. For many problems, a simplified 2D theory captures phenomena of interest. One dimension is ignored consistent with the full 3D equations. This practice has been widely and profitably applied in fluid mechanics, partly because of the complexity associated with 3D analysis and computation, but furthermore to develop exact simplified solutions and structures. A handful of 2D models (e.g. [13]) has been applied to model or predict unexplained behavior of macromolecular materials such as LCPs. We first point out the lack of correspondence between posited low-dimensional orientation tensor theories and the 3D theory. We then show how to self-consistently extract orientation structures from the bonafide 3D theory corresponding to "planar" or unidirectional variations in order parameters and/or optical axes. This paper serves as a caution for the use of low-dimensional flow–orientation models, in that the restriction of the orientation tensor from 3D to lower dimensions requires care to preserve consistency with the full equations. This caution duly noted, we proceed to show how to construct analogs of exact 3D low-dimensional structures with the formal 2D theory. These analogies suggest intuitive value of the 2D theory, and predictions such as those in [13].

2. Doi–Marrucci–Greco theory

We briefly review the Doi theory extended by Marrucci and Greco for nonhomogeneous LCPs [18]. This theory couples three important nematic effects:

- a short-range excluded-volume potential (of Maier–Saupe form) which resolves the homogeneous phase transitions of nematics [1];
- a nonlocal intermolecular potential accounting for intermediate-range elastic coupling, which resolves the energy cost for spatial distortions analogous to Frank elasticity;
- the additional effect of the molecular aspect ratio, p, of the major and minor axes of an oblate spheroid ($p = 0$ for a circular disk, $p = 1$ for a sphere, $p = \infty$ for a rod of vanishing cross section); this geometric parameter has been shown to be necessary to resolve important tumbling and aligning behavior of flowing nematic LCPs [8,12].

In the following description, bold variables with lower case letters represent vectors of dimension $d = 2$ or 3, bold capital letters are tensors with $d \times d$ matrix representations, and non-bold letters represent scalar fields or parameters. We present the model equations for flows, though our explicit solutions are focused on pure nematic structures for this paper. This approach provides a foundation for the significantly more complex phenomena associated with full flow–orientation interactions.

Fix the space dimension $d = 2$ or 3. Let $f(\mathbf{m}, \mathbf{x}, t)$ be the probability density function corresponding to the probability that an arbitrary oblate spheroid-shaped polymer molecule is in direction $\mathbf{m}$ ($\|\mathbf{m}\| = 1$) at location $\mathbf{x}$ and time t. The central piece of the DMG theory is the kinetic equation for the probability density function $f(\mathbf{m}, \mathbf{x}, t)$, given as follows with translational spatial diffusion effects neglected:

$$\text{(a)}\quad \frac{\mathrm{D}f}{\mathrm{D}t} = \frac{1}{6\lambda}\left(\frac{\partial}{\partial \mathbf{m}} \cdot \frac{\partial}{\partial \mathbf{m}} f\right) - \frac{\partial}{\partial \mathbf{m}} \cdot \left\{[\dot{\mathbf{m}}] f - \frac{1}{6kT\lambda}\left(\frac{\partial}{\partial \mathbf{m}} V\right) f\right\},$$

$$\text{(b)}\quad \dot{\mathbf{m}} = \boldsymbol{\Omega} \cdot \mathbf{m} - a[\mathbf{D} \cdot \mathbf{m} - \mathbf{D} : \mathbf{mmm}], \tag{1}$$

where $\mathbf{D}$ and $\boldsymbol{\Omega}$ are the rate of strain and vorticity tensors, respectively,

$$\mathbf{D} = \tfrac{1}{2}(\boldsymbol{\nabla}\mathbf{v} + \boldsymbol{\nabla}\mathbf{v}^{\mathrm{t}}), \qquad \boldsymbol{\Omega} = \tfrac{1}{2}(\boldsymbol{\nabla}\mathbf{v} - \boldsymbol{\nabla}\mathbf{v}^{\mathrm{t}}), \tag{2}$$

where $\mathbf{v}$ is the associated velocity vector field for a flowing LCP; $a = (p^2 - 1)/(p^2 + 1)$, where p is the molecular aspect ratio, so that $-1 \le a \le 1$, $a = 1, 0, -1$ correspond to the shape of the LCP molecule as a rigid rod, sphere and circular disk, respectively, λ the elastic relaxation time, assumed constant, that gives the rate $1/\lambda$ at which the molecule returns to a stable homogeneous equilibrium when perturbed from it, k the Boltzmann constant, T the absolute temperature, $(\mathrm{D}/\mathrm{D}t)(\cdot)$ denotes the material derivative $(\partial/\partial t)(\cdot) + \mathbf{v} \cdot \boldsymbol{\nabla}(\cdot)$. The Marrucci–Greco potential [18] V in Eq. (1) is given by a scalar contraction of a molecular-scale tensor ($\mathbf{m} \otimes \mathbf{m}$) with a mesoscopic tensor ($\mathbf{Q}_l$):

$$\text{(a)}\quad V = -\frac{3}{2}NkT\left(\mathbf{m} \otimes \mathbf{m} - \frac{\mathbf{I}}{d}\right) : \mathbf{Q}_l, \qquad \text{(b)}\quad \mathbf{Q}_l = \left(1 + \frac{l^2}{24}\Delta\right)\left\langle \mathbf{m} \otimes \mathbf{m} - \frac{\mathbf{I}}{d}\right\rangle, \tag{3}$$

where Δ is the Laplacian, $\Delta = \boldsymbol{\nabla} \cdot \boldsymbol{\nabla}$, and l the persistence length of the distortional elasticity interaction. For $l = 0$, the potential V reduces to the Maier–Saupe potential for homogeneous excluded-volume interactions; the terms proportional to l are the Marrucci–Greco distortional elasticity potential. The bracket $\langle\,\rangle$ denotes an average over all possible molecular directions at $(\mathbf{x}, t)$ with respect to the probability density function:

$$\langle(\cdot)\rangle = \int_{\|\mathbf{m}\|=1} (\cdot) f(\mathbf{m}, \mathbf{x}, t)\, \mathrm{d}\mathbf{m}. \tag{4}$$

Here N is a dimensionless form of the polymer number density c, a fundamental experimental parameter, since both potentials depend strongly on the concentration which varies inversely with temperature. If one restricts to homogeneous nematics, i.e. $l^2 = 0$ in (3), suppresses flow ($\mathbf{v} = \mathbf{0}$), then the Doi theory successfully describes the

classical phase transitions of nematic LCPs through the single control parameter N (see [1–3,6,10,11]). The DMG theory is derived for $d = 3$, but the theory formally extends to $d = 2$; their correspondence will be discussed below.

Notational remarks. Recall standard tensor algebra

$$\mathbf{m} \otimes \mathbf{m} = \mathbf{m}\mathbf{m}^{\mathrm{t}}, \qquad \mathbf{A} : \mathbf{B} = \mathrm{tr}(\mathbf{A}\mathbf{B}^{\mathrm{t}}), \tag{5}$$

and $\mathbf{A} \cdot \mathbf{B}$ or $\mathbf{AB}$ is the standard matrix multiplication.

From this kinetic theory, one can derive continuum models for the mesoscopic, or average, internal orientation properties of nematic LCPs, the simplest of which involves the average (defined by (4)) of the second moment of the molecule direction $\mathbf{m}$, normalized to a symmetric, traceless tensor $\mathbf{Q}$,

$$\mathbf{Q} = \langle \mathbf{m} \otimes \mathbf{m} \rangle - \frac{\mathbf{I}}{d}, \qquad \mathrm{tr}(\mathbf{Q}) = 0. \tag{6}$$

To derive a mesoscale theory for $\mathbf{Q}$ coupled to flow, the definitions (4) and (6), molecular dynamics (1)b and Smoluchowski equation (1)a lead one to the classic nonlinear closure problem, with second moments coupling to fourth moments. If one adopts the Doi quadratic closure rule $\langle \mathbf{m} \otimes \mathbf{m} \otimes \mathbf{m} \otimes \mathbf{m} \rangle \approx \langle \mathbf{m} \otimes \mathbf{m} \rangle \langle \mathbf{m} \otimes \mathbf{m} \rangle$ [5,6], we arrive at the mesoscale, *orientation tensor equation*:

$$\begin{aligned}
&\frac{\mathrm{d}}{\mathrm{d}t}\mathbf{Q} - \boldsymbol{\Omega}\mathbf{Q} + \mathbf{Q}\boldsymbol{\Omega} - a[\mathbf{D}\mathbf{Q} + \mathbf{Q}\mathbf{D}] = \frac{2a}{d}\mathbf{D} - 2a\mathbf{D} : \mathbf{Q}\left(\mathbf{Q} + \frac{\mathbf{I}}{d}\right) - \frac{1}{\lambda}[\mathbf{F}(\mathbf{Q}) + \mathbf{E}(\mathbf{Q})],\\
&\mathbf{F}(\mathbf{Q}) = \left(1 - \frac{N}{d}\right)\mathbf{Q} - N(\mathbf{Q}\mathbf{Q}) + N(\mathbf{Q} : \mathbf{Q})\left(\mathbf{Q} + \frac{\mathbf{I}}{d}\right),\\
&\mathbf{E}(\mathbf{Q}) = -\frac{Nl^2}{24}\left[\frac{1}{d}\Delta\mathbf{Q} + \frac{1}{2}\Delta\mathbf{Q}\mathbf{Q} + \frac{1}{2}\mathbf{Q}\Delta\mathbf{Q} - (\Delta\mathbf{Q} : \mathbf{Q})\left(\mathbf{Q} + \frac{\mathbf{I}}{d}\right)\right].
\end{aligned} \tag{7}$$

Note that $\mathbf{F}(\mathbf{Q})$ is the effective mesoscale, tensorial field arising from the scalar Maier–Saupe excluded-volume potential (3)a, and $\mathbf{E}(\mathbf{Q})$ the tensorial field arising from the distortional Frank elasticity effect (3)b. For flows, one must derive the flow–nematic stress tensor τ.

A nonlocal virtual work argument along with the quadratic closure rule [6,8] give the flow–orientation constitutive relation for the stress tensor:

$$\begin{aligned}
\tau = {} & 2\eta\mathbf{D} + 3ackT\left[\mathbf{Q} - \frac{N}{2}\left(\left(\mathbf{I} + \frac{l^2}{24}\Delta\right)\mathbf{Q}\left(\mathbf{Q} + \frac{\mathbf{I}}{d}\right) + \left(\mathbf{Q} + \frac{\mathbf{I}}{d}\right)\left(\mathbf{I} + \frac{l^2}{24}\Delta\right)\mathbf{Q}\right)\right.\\
& \left. + N\left(\mathbf{I} + \frac{l^2}{24}\Delta\right)\mathbf{Q} : \mathbf{Q}\left(\mathbf{Q} + \frac{\mathbf{I}}{d}\right)\right] + \frac{cNkTl^2}{16}[\mathbf{Q}\Delta\mathbf{Q} - \Delta\mathbf{Q}\mathbf{Q}] - \frac{cNkTl^2}{32}[\nabla\mathbf{Q} : \nabla\mathbf{Q} - (\nabla\nabla\mathbf{Q}) : \mathbf{Q}]\\
& + 3ckT\left[\zeta_1(a)(\mathbf{Q}\mathbf{D} + \mathbf{D}\mathbf{Q}) + \zeta_2(a)\mathbf{D} : \mathbf{Q}\left(\mathbf{Q} + \frac{\mathbf{I}}{d}\right)\right],
\end{aligned} \tag{8}$$

where the new parameters are: η is the Newtonian isotropic viscosity, c the number of polymer molecules per unit volume, and $3ckT\zeta_1(a)$ and $3ckT\zeta_2(a)$ the viscosity parameters due to polymer–solvent interaction.

To complete this system, one adjoins the *balance of linear momentum*:

$$\rho\frac{\mathrm{d}\mathbf{v}}{\mathrm{d}t} = \nabla \cdot (-p\mathbf{I} + \tau), \tag{9}$$

where ρ is the fluid density and p the scalar pressure. We further assume the flow is incompressible so that $\mathbf{v}$ satisfies the *continuity equation*:

$$\nabla \cdot \mathbf{v} = 0. \tag{10}$$

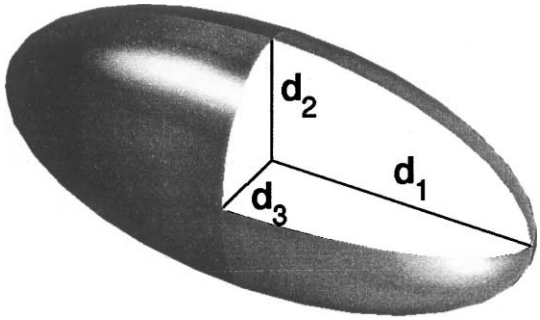

Fig. 1. A geometric representation of the mesoscale orientation tensor $\mathbf{Q}$. The axes lengths d_i are given by eigenvalues $(d_i - \frac{1}{3})$ of $\mathbf{Q}$, whereas the axes are given by the orthonormal frame of eigenvectors of $\mathbf{Q}$.

The orientation tensor equation (7), constitutive equation for the extra stress (8), balance of linear momentum (9) and the continuity equation (10) constitute the mesoscale DMG model for LCPs, which couples flow $\mathbf{v}$ and the mesoscopic molecular orientation tensor $\mathbf{Q}$. The eigenvalues of $\mathbf{Q}$, $d_i - \frac{1}{3}$, are the order parameters, which convey the averaged degrees of orientation with respect to the eigenvectors of $\mathbf{Q}$, $\mathbf{n}_i$, which are the mesoscopic principal optical axes (Fig. 1). This information constitutes a spectral representation of $\mathbf{Q}$:

$$\mathbf{Q} = \sum_{i=1}^{3} \left(d_i - \frac{1}{3} \right) \mathbf{n}_i \otimes \mathbf{n}_i, \qquad \sum_{i=1}^{3} d_i = 1, \quad d_i = \langle \mathbf{n}_i \cdot \mathbf{m} \rangle = \langle \cos^2 \langle \mathbf{n}_i, \mathbf{m} \rangle \rangle, \tag{11}$$

where $\langle \mathbf{n}_i, \mathbf{m} \rangle$ denotes the angle between the directions $\mathbf{n}_i$ and $\mathbf{m}$. The isotropic state corresponds to $d_i = \frac{1}{3}$, $i = 1, 2, 3$, or $\mathbf{Q} = \mathbf{0}$, and the ellipsoid of Fig. 1 reverts to a sphere with random mesoscale order. The experimentalist probes the optical axes by varying the plane transverse to the light signal; the principal axes correspond to a plane with local maximal birefringence. Birefringence (or anisotropy) in the plane of $\mathbf{n}_i$, $\mathbf{n}_j$ (or any plane) is measured by differences in the principal degrees of orientation, $B_{ij} = |d_i - d_j|$. Note further that $d_i > \frac{1}{3}$ implies that on an average the molecules align toward the principal axis $\mathbf{n}_i$, whereas $d_i < \frac{1}{3}$ implies greater alignment with the plane normal to $\mathbf{n}_i$.

3. Cautionary notes on the correspondence between $d = 2$ and 3 nematic tensor theories

It is customary in fluid mechanics to study low-dimensional flows. The Navier–Stokes equations are recovered from (9) and (10) with $\mathbf{Q} = \mathbf{0}$, which clearly self-consistently restrict from $d = 3$ to 2. More importantly, any solution of the Navier–Stokes equation for $d = 2$ generates a solution of the 3D fluid equations. Here we point out the flow–orientation system (7)–(10) for $d = 2$ and 3 fails to have an analogous correspondence.

We show first from definition (6) that there is no clear relationship between the 3D tensor $\mathbf{Q}_{3\times3}$ and the 2D tensor $\tilde{\mathbf{Q}}_{2\times2}$ that is inherited from a "planar" molecule $\mathbf{m} = (\tilde{\mathbf{m}}, 0)$, where $\tilde{\mathbf{m}}$ is a unit 2 vector. [1] (We use "˜" overbars to label 2D vectors and tensors, e.g., $\mathbf{I}_{3\times3} = \mathbf{I}$, $\mathbf{I}_{2\times2} = \tilde{\mathbf{I}}$.) From $\tilde{\mathbf{m}}$, we construct $\tilde{\mathbf{Q}}$,

$$\tilde{\mathbf{Q}} = \langle \tilde{\mathbf{m}} \otimes \tilde{\mathbf{m}} \rangle - \tfrac{1}{2}\tilde{\mathbf{I}}. \tag{12}$$

[1] All vectors are presumed column vectors.

With $\mathbf{m} = (\tilde{\mathbf{m}}, 0)$, we construct the relationship between $\mathbf{Q}$ and $\tilde{\mathbf{Q}}$:

$$\mathbf{Q} = \langle \mathbf{m} \otimes \mathbf{m} \rangle - \frac{\mathbf{I}}{3} = \begin{bmatrix} \tilde{\mathbf{Q}} + \frac{1}{6}\tilde{\mathbf{I}} & \mathbf{0}_{2\times 1} \\ \mathbf{0}_{1\times 2} & -\frac{1}{3} \end{bmatrix}. \tag{13}$$

Naively one might suspect that insertion of (13) into the nematic equation (7) with $d = 3$ will produce the corresponding $d = 2$ equation for $\tilde{\mathbf{Q}}$. A straightforward calculation shows the $(3, 3)$ component of this tensor equation has a contradiction with or without flow, arising from the linear term in $F(\mathbf{Q})$. This term corresponds in the kinetic theory to rotational Brownian motion of the rod-like molecules, referred to as rotary diffusion. Conversely, if one has a solution $\tilde{\mathbf{Q}}$ for the $d = 2$ equation (7), there is no corresponding solution $\mathbf{Q}$ for the $d = 3$ equation (7) by the relation (13).

The upshot of these observations is that solutions of the 2×2 tensor theory (7) with $\mathbf{Q}$ formally replaced by $\tilde{\mathbf{Q}}$ do not yield special low-dimensional 3D solutions of (7). There is no apparent relationship that produces a 3D solution $\mathbf{Q}$ from a 2D solution $\tilde{\mathbf{Q}}$. This result serves as a caution for the interpretation of phenomena derived from a posited 2D theory [13]; they do not directly correspond to "planar orientation structures".

As a result of these observations, one has to posit special representations of $\mathbf{Q}$ which have the effect of restricting dimensionality of orientation tensor degrees of freedom. Indeed, historically this was accomplished by positing a director theory at the mesoscale, which is the limit of (11) corresponding to a uniaxial tensor $\mathbf{Q}$, for which two eigenvalues are equal, say $d_1 = d_2$, the distinguished eigenvector ($\mathbf{n} = \mathbf{n}_3$) of the simple eigenvalue (d_3) is called the uniaxial director, or optical axis. This class of tensors assumes isotropic orientation in the plane transverse to the distinguished directors; in this sense the mesoscale geometry mimics the molecular geometry of a prolate ellipsoid for $\frac{1}{3} < d_3 < 1$, a sphere for $d_3 = \frac{1}{3}$, and an oblate ellipsoid for $0 \leq d_3 < \frac{1}{3}$. The uniaxial class of 3D tensors admits a simplified form of (11),

$$\mathbf{Q} = s(\mathbf{n} \otimes \mathbf{n} - \tfrac{1}{3}\mathbf{I}), \quad s = \tfrac{1}{2}(3d_3 - 1). \tag{14}$$

One can seek restricted behavior of s and $\mathbf{n}$, e.g. they only vary in (x, y), or in x. We note that historically the liquid crystal continuum theories of Frank, Leslie, Ericksen, et al. consisted of equations for a uniaxial director $\mathbf{n}$, which implicitly asserts $s = 1$, or $d_3 = 1$, i.e. perfect alignment of molecules $\mathbf{m}$ and the mesoscale axis $\mathbf{n}$. Later, Ericksen realized the need to couple the order parameter s, or degree of molecular orientation with respect to the mesoscale director $\mathbf{n}$. This evolution of the Leslie–Ericksen–Frank director theory was mirrored by the completely independent development of Doi–Edwards–de Gennes et al. which naturally leads to a full tensorial mesoscale order parameter, $\mathbf{Q}$.

In our analysis to follow, we develop other ways to impose dimensionality restrictions on $\mathbf{Q}$, relying on the geometric intuition afforded by Fig. 1. For example, one might fix one director parallel to $\mathbf{e}_z$, allowing the remaining orthogonal pair of optical axes to vary arbitrarily in the (x, y)-plane. Then one has to determine how the order parameters vary consistent with the dynamics (7)–(10). The intuition we follow is that of "separating" the structure of $\mathbf{Q}$ in spectral coordinates, i.e., directors and order parameters, rather than in coordinate matrix representations. Remarkably, this geometric picture, in which eigenvalues and eigenvectors of $\mathbf{Q}$ depend either on complementary space, time coordinates, or together on a low-dimensional subset of x, t, yields a rich variety of exact solutions. These constructions generalize recent results of the authors [11].

4. Spatial structures of the 3D DMG model without flow

We now construct various special solutions of the 3D DMG model with effective planar or 1D structure, with flow suppressed.

4.1. Biaxial orientation patterns corresponding to transversely varying order parameters and director fields

We seek solutions of the 3D DMG model satisfying the following spectral conditions:

- two directors ($\mathbf{n}$ and $\mathbf{n}^\perp$) are confined parallel to the xy-plane yet allowed to vary in a transverse yz-plane;
- the third director is constrained $\mathbf{n}_3 = \mathbf{e}_z$;
- the director variation is steady;
- the order parameters (s, β) are allowed to vary in time (t) and along the x-direction of director homogeneity:

$$\mathbf{Q} = s(x,t)(\mathbf{n}(y,z) \otimes \mathbf{n}(y,z) - \tfrac{1}{3}\mathbf{I}) + \beta(x,t)(\mathbf{e}_z \otimes \mathbf{e}_z - \tfrac{1}{3}\mathbf{I}). \tag{15}$$

The two independent order parameters are given in terms of the degrees of orientation, (11), by

$$s = d_1 - d_2, \qquad \beta = 1 - d_1 - 2d_2. \tag{16}$$

Motivated by the presence of the Laplacian operator in the orientation tensor equation, we require $\mathbf{n}$ to satisfy the equations:

$$\begin{aligned} &\left(\frac{\partial^2}{\partial y^2} + \frac{\partial^2}{\partial z^2}\right)\mathbf{n} = -\gamma^2\mathbf{n}, \quad \gamma^2 = \gamma_1^2 + \gamma_2^2, \quad \frac{\partial}{\partial y}\mathbf{n} = \gamma_1\mathbf{n}^\perp, \\ &\frac{\partial}{\partial z}\mathbf{n} = \gamma_2\mathbf{n}^\perp, \quad \frac{\partial}{\partial y}\mathbf{n}^\perp = -\gamma_1\mathbf{n}, \quad \frac{\partial}{\partial z}\mathbf{n}^\perp = -\gamma_2\mathbf{n}, \end{aligned} \tag{17}$$

where γ_1, γ_2 are constants. With the directors obeying (17), the full tensor PDE (7) with $\mathbf{D} = \mathbf{0}$ and $\mathbf{\Omega} = \mathbf{0}$ reduces to two coupled reaction–diffusion equations for the order parameters s, β:[2]

$$\begin{aligned} s_t = &-\frac{1}{\lambda}\left[V(s) + \frac{2N}{3}s\beta(1+\beta-s) - \frac{Nl^2\gamma^2}{36}(-s^2+3s^3+2s\beta-2s)\right] \\ &+\frac{Nl^2}{72\lambda}[(1-s)(1+2s-\beta)s_{xx} - s(1+2\beta-s)\beta_{xx}], \\ \beta_t = &-\frac{1}{\lambda}\left[V(\beta) + \frac{2N}{3}s\beta(1+s-\beta) - \frac{Nl^2\gamma^2}{36}s(s+3s\beta+\beta-1)\right] \\ &+\frac{Nl^2}{72\lambda}[(1-\beta)(1+2\beta-s)\beta_{xx} - \beta(1+2s-\beta)s_{xx}], \end{aligned} \tag{18}$$

where

$$V(s) = s(1 - \tfrac{1}{3}N(1-s)(2s+1)), \tag{19}$$

which has zeros $s_0 = 0$, $s_\pm = \frac{1}{4}(1 \pm \sqrt{1 - 8/3N})$. We note that $\int V(s)\,\mathrm{d}s$ is the bulk free energy in the homogeneous uniaxial phase.

One family of solutions of (17) is

$$\mathbf{n} = \begin{pmatrix} \cos\theta \\ \sin\theta \\ 0 \end{pmatrix}, \qquad \mathbf{n}^\perp = \begin{pmatrix} -\sin\theta \\ \cos\theta \\ 0 \end{pmatrix}, \quad \theta = \gamma_1 y + \gamma_2 z + \theta_0, \tag{20}$$

where θ_0 is a constant, and the wave vector $(0, \gamma_1, \gamma_2)$ is arbitrary in the yz-plane.

[2] Note that (18) differs from the equations in [11] where we used $\mathbf{n}^\perp$ instead of $\mathbf{n}$ in the expression (15).

Note the director variation is coupled to the order parameter structure only through the wave number γ. In the limit $\gamma_1 = \gamma_2 = 0$, the directors are constant and we recover exact order parameter-induced patterns presented in [11]. This two parameter (γ_1, γ_2) family of solutions captures both "sinuous" optical axes restricted to a plane and nontrivial order parameter variations transverse to that plane. We now detail special classes of behavior within this family.

4.1.1. Patterns with planar periodic optical axes and homogeneous order parameters

If we restrict the order parameter PDEs (18) to constant steady states, we recover a minor simplification of the family of oscillatory patterns derived in [11]. That is, if $s,\ \beta$ are independent of x, then one can extend (17) and (20) to allow full (x, y, z) variation of $\mathbf{n},\ \mathbf{n}^{\perp}$, with corresponding wave vector $\gamma = (\gamma_1, \gamma_2, \gamma_3)$, and $\theta(x, y, z) = \gamma \cdot \mathbf{x} + \theta_0$. Otherwise, the structure is identical, and the order parameter equilibria (s^*, β^*) of (18) are roots of two simultaneous cubic polynomials:

$$V(s) + \tfrac{2}{3}Ns\beta(1 + \beta - s) - \tfrac{1}{36}Nl^2\gamma^2(-s^2 + 3s^3 + 2s\beta - 2s) = 0,$$

$$V(\beta) + \tfrac{2}{3}Ns\beta(1 + s - \beta) - \tfrac{1}{36}Nl^2\gamma^2 s(s + 3s\beta + \beta - 1) = 0. \tag{21}$$

The coupling constant, $l^2\gamma^2$, parameterizes distortional elasticity arising through cubic polynomial terms in (s, β). The remaining terms are excluded-volume effects, also cubic polynomials. Therefore, these competing potentials balance for this family of patterns, and both lead to bifurcation behavior as the material parameters (N, l) and pattern parameters (γ) vary.

For $l\gamma = 0$, excluded-volume effects with a quartic Maier–Saupe potential (leading to $F(\mathbf{Q})$ in (7)) imply the only equilibria are uniaxial [10], lying along the order parameter subspaces $\beta = 0,\ s = 0,\ s = \beta$.

The elasticity terms identically vanish along the special uniaxial subspace $s = 0$, for which the uniaxial director is $\mathbf{e}_z$. Thus the simple uniaxial family $(s, \beta) = (0, \beta_j),\ \beta_j = 0,\ \frac{1}{4}(1 \pm \sqrt{1 - 8/3N})$ persists for all l and γ. These orientation patterns are homogeneous since the oscillatory directors $\mathbf{n},\ \mathbf{n}^{\perp}$ lie in the plane of isotropy of $\mathbf{Q}$; the formula (24) also shows the dependence on $\mathbf{n}$ is annihilated when $s = 0$. These equilibrium branches are depicted in Fig. 2b.

All other roots (s, β) of (21) correspond to patterns that are both fully biaxial and spatially periodic. Thus planar periodic variation of the optical axes, (20), forces full biaxial structure in which the degrees of orientation, $d_1,\ d_2,\ d_3$, equations (11), with respect to $\mathbf{n},\ \mathbf{n}^{\perp},\ \mathbf{e}_z$, respectively, are all distinct. For fixed $l = 0.15$, and $(\gamma_1, \gamma_2) = (6, 8),\ |\gamma| = 10$, Fig. 2 depicts all roots (s^*, β^*) of (21) for $0 < N < 10$. Fig. 3 depicts a typical planar (y, z) light intensity pattern that would result from a light scattering experiment applied to this mesoscale orientation field, where we have chosen $N = 4$, wave vector $\gamma = (\gamma_1, \gamma_2) = (6, 8),\ |\gamma| = 10,\ l = 0.15$. Note that experimentalists use light scattering data to infer birefringence patterns [4,19], whereas we are predicting the intensity patterns from the exact birefringence of our solutions; see the caption of Fig. 3 for the precise formula from [19]. As $l\gamma$ increases from 0, some equilibrium branches depicted in Fig. 2 either move out of the triangular range (see Fig. 2b) of order parameter values and are unphysical, or the branches terminate by becoming non-real (see Fig. 4). This numerical observation implies a bound for each biaxial branch

$$\gamma l < \Gamma, \tag{22}$$

which physically implies the wavelengths of director variation, $2\pi/\gamma_1$ and $2\pi/\gamma_2$, must exceed a minimum value that scales with the persistence length l. This result is intuitively reasonable in that the sinuous director pattern requires several persistence lengths of the distortional elasticity pattern that supports it. An analogous minimum thickness condition in the direction transverse to the director variations has been derived by Pergamenshchik [21] due to surface elasticity potentials in thin nematic layers.

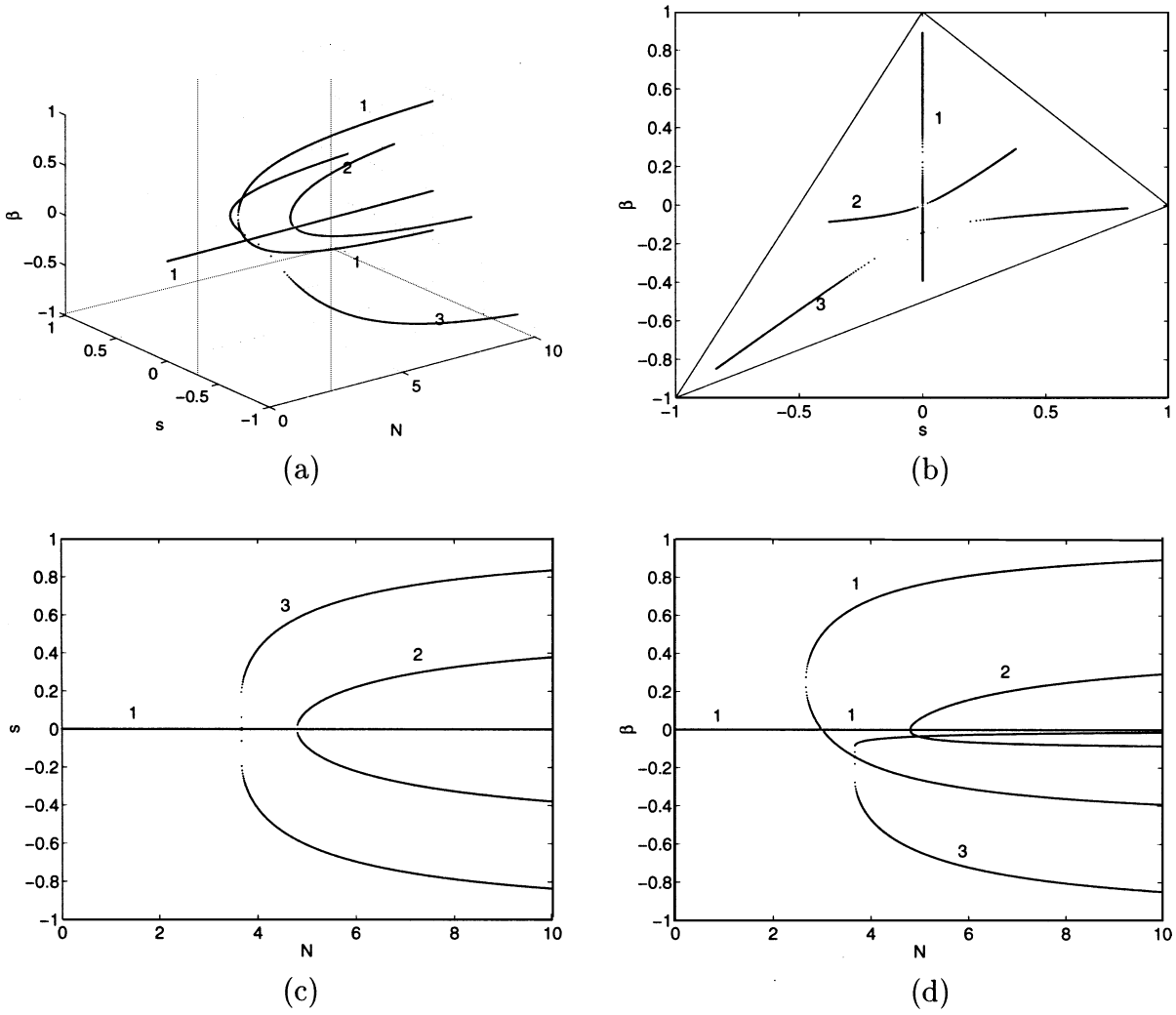

Fig. 2. Homogeneous order parameter equilibria of Eq. (18) for LCP concentration range $0 < N < 10$, with $\gamma = 10$, $l = 0.15$. The bifurcation diagram in (a) (N, s, β); (b) (s, β); (c) (N, s); (d) (N, β). At a critical concentration ($N = 3.75$), there is a pitchfork bifurcation from the oblate branch $(0, \frac{1}{4}(1 - 3\sqrt{1 - 8/3N})$, yielding two biaxial equilibrium branches. At another critical concentration ($N = 5$), a second pitchfork bifurcation occurs along the isotropic branch giving rise to two other biaxial equilibrium families.

4.1.2. Patterns with periodic optical axes coupled with transverse order parameter modulations

We now illustrate (Fig. 5) oscillating (in x) order parameter behavior of (18), which occurs transverse to the planar (y, z) double periodicity of the optical axes. If the x-direction is associated with a layer thickness of at least one quasi-period of (s, β), and light scattering experiments are done with rays along the x-direction, then the intensity plots will average out the order parameter variations. We conclude that a standard experimental arrangement will not distinguish this pattern (Fig. 5) from the co-existing patterns (Fig. 3b) with identical sinuous optical axes but fixed (constant) biaxial order parameter values.

We have illustrated with these exact pattern constructions that the DMG tensor PDE admits hierarchies of co-existing "separable solutions" in spectral variables. These families are but one example of a geometric

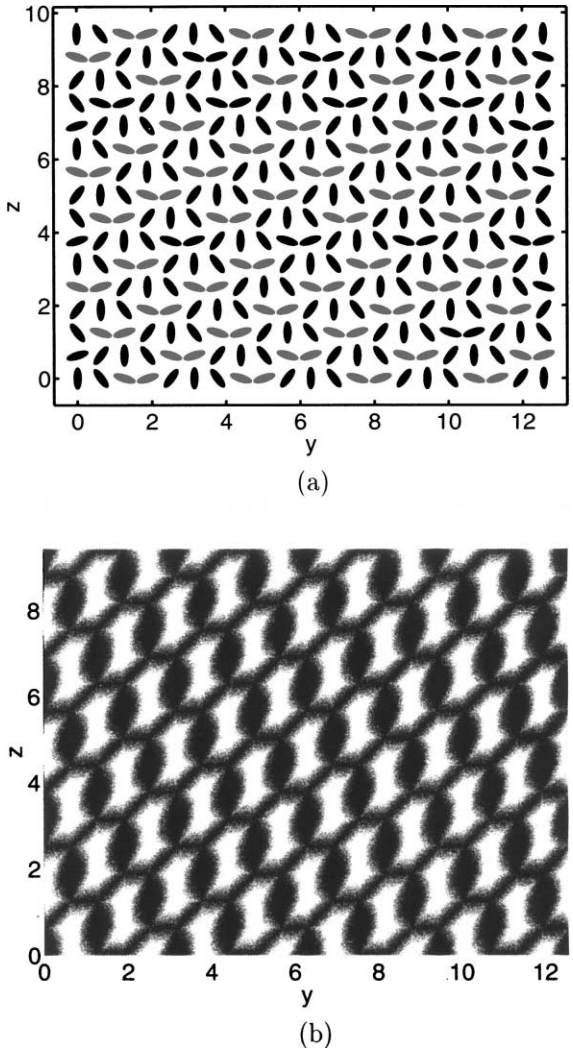

Fig. 3. (a) Doubly periodic array of the projection of the orientation tensor "ellipsoid" onto the yz-plane. The ellipsoid is constructed with major axes given by the orthonormal frame of directors $\mathbf{n}$ and $\mathbf{n}^{\perp}$, (20), of $\mathbf{Q}$, which lie in the xy-plane but vary periodically in the yz-plane. The axis lengths of the ellipses are given by the degrees of orientation, d_i, with respect to the directors. For the fixed order parameter values $s = -0.4171,\ \beta = -0.4703$, of equations (21), corresponding to $N = 4,\ \gamma = 10,\ l = 0.15,\ d_1 = 0.1588,\ d_2 = 0.2120,\ d_3 = 0.6292$. (b) A light intensity pattern corresponding to (a) for $\gamma = (6, 8)$. The light intensity function [11] is defined as $I = I_0 \sin^2(2\pi a B) \sin^2(2\theta)$, where a is the ratio of the sample thickness to the wavelength of incident light, B is the birefringence, $B = |d_2 - d_3|,\ \theta = \gamma_1 y + \gamma_2 z$.

factorization in which the directors and order parameters depend on complementary coordinates. For example, another family of separable solutions can be constructed from the ansatz

$$\mathbf{Q} = s(x, z, t)(\mathbf{n}(y) \otimes \mathbf{n}(y) - \tfrac{1}{3}\mathbf{I}) + \beta(x, z, t)(\mathbf{e}_z \otimes \mathbf{e}_z - \tfrac{1}{3}\mathbf{I}), \tag{23}$$

interchanging the 2D and 1D spatial variations. We defer these solutions to another context.

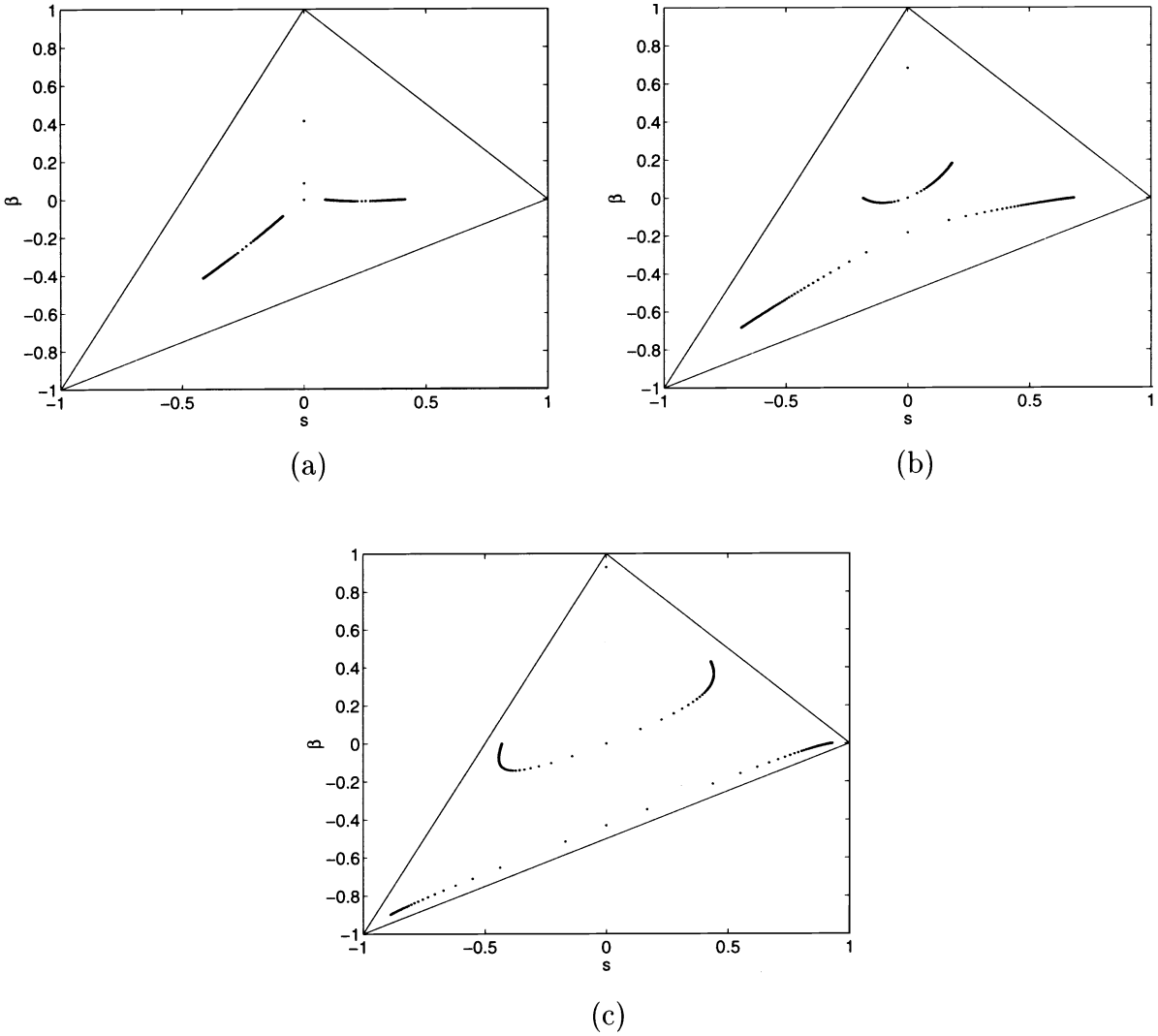

Fig. 4. The spatially homogeneous equilibria of (21) for $0 < \gamma l < \Gamma$ with three different values of N. (a) $N = 2.8$. At approximately $\gamma l = \Gamma = 0.71$, all four branches terminate. (b) $N = 4$. At approximately $\gamma l = \Gamma = 1.494$, the two branches originating from the oblate phase collide at the isotropic phase and terminate; at approximately $\gamma l = \Gamma = 2.044$, the other two branches coming out of the highly aligned prolate phase collide at an oblate phase and terminate. (c) $N = 15$. The analogous scenario occurs at $\gamma l = \Gamma = 2.6678$ and $\gamma l = \Gamma = 2.84$, respectively.

4.2. Biaxial orientation patterns with coupled order parameter and director variation along a single direction

We seek patterns whose directors and order parameters vary along a single direction (x),

$$\mathbf{Q} = s(x,t)(\mathbf{n}(x,t) \otimes \mathbf{n}(x,t) - \tfrac{1}{3}\mathbf{I}) + \beta(x,t)(\mathbf{e}_z \otimes \mathbf{e}_z - \tfrac{1}{3}\mathbf{I}), \tag{24}$$

where $\mathbf{n} = (\cos(\xi(x,t)),\ \sin(\xi(x,t)), 0)^{\mathrm{T}}$. We again restrict the variable optical axes, $\mathbf{n}$ and $\mathbf{n}^{\perp}$, to the xy-plane. The orientation tensor equation reduces to

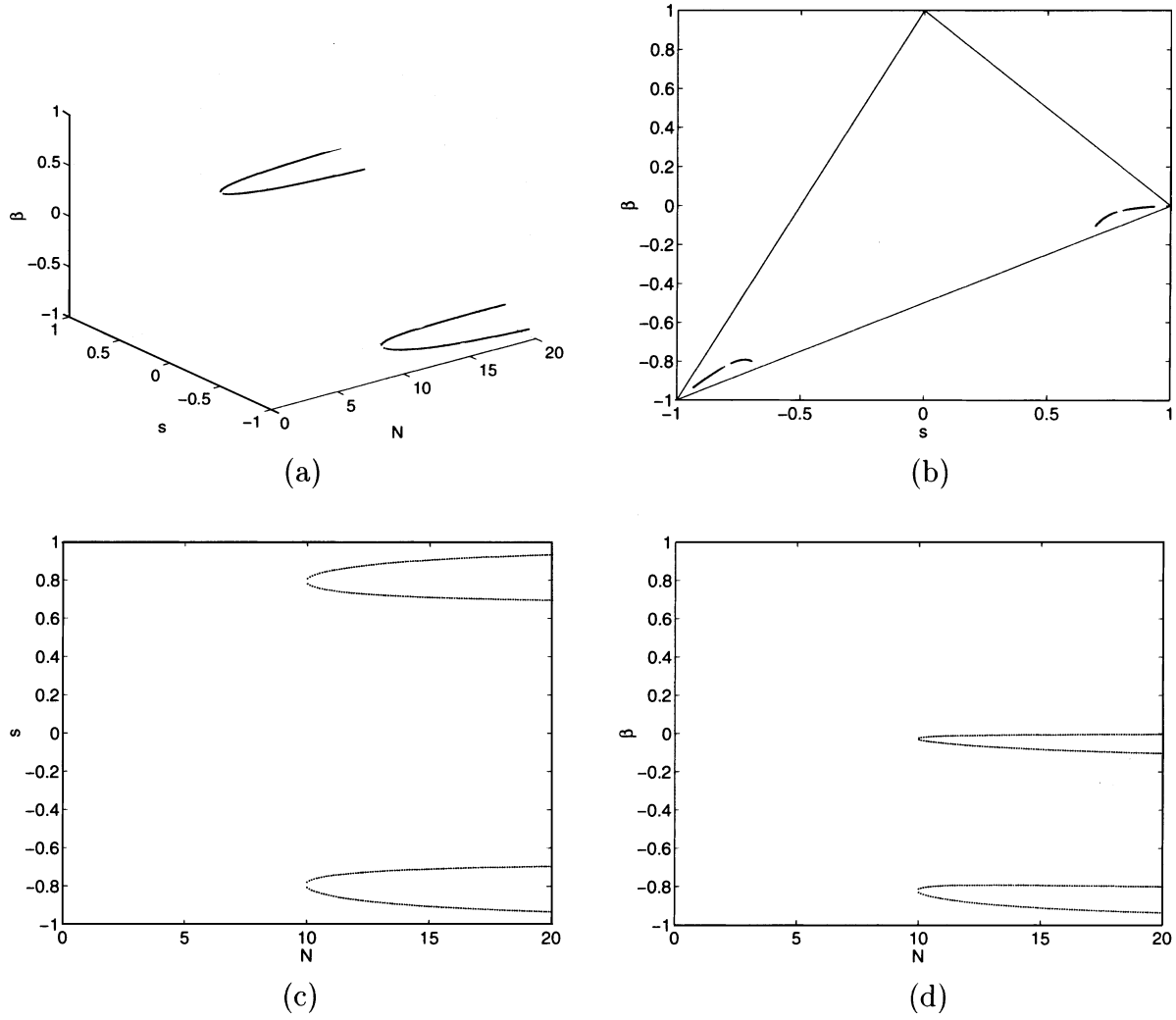

Fig. 5. The spatially homogeneous equilibria of (28) for $0 < N < 20$ with $C = 10$, $l = 0.3464$. The bifurcation diagram in: (a) (N, s, β); (b) (s, β); (c) (N, s); (d) (N, β).

$$
\begin{aligned}
s_t &= -\frac{\sigma}{\lambda}\left[V(s) + \frac{2N}{3}s\beta(1+\beta-s) + \frac{Nl^2}{36}(s^2 - 3s^3 + 2s - 2s\beta)\xi_x^2\right] \\
&\quad + \frac{\sigma N l^2}{72\lambda}[(1-s)(1+2s-\beta)s_{xx} - (1+2\beta-s)s\beta_{xx}], \\
\beta_t &= -\frac{\sigma}{\lambda}\left[V(\beta) + \frac{2N}{3}s\beta(1+s-\beta) + \frac{Nl^2}{36}(-s^2 - s\beta + s - 3s^2\beta)\xi_x^2\right] \\
&\quad + \frac{\sigma N l^2}{72\lambda}[-\beta(1+2s-\beta)s_{xx} + (1-\beta)(1+2\beta-s)\beta_{xx}], \\
\xi_t &= \frac{\sigma N l^2}{144\lambda s}[(-4\beta s_x + 2s s_x + 4s_x)\xi_x + (-2s\beta + 2s + s^2)\xi_{xx}].
\end{aligned} \tag{25}
$$

In steady state, the director variable ξ satisfies

$$\left(1+\frac{2(1-\beta)}{s}\right)[s^2\xi_x]_x = 0, \tag{26}$$

so that

$$\xi_x = \frac{C}{s^2}. \tag{27}$$

The integration constant C is somehow determined by the available energy required to sustain the variation in optical axes; the initial phase $\xi(0)$ is arbitrary. Substituting (27) into (25), we obtain a closed steady-state system for the order parameters (s, β):

$$\begin{aligned}
0 &= -\frac{1}{\lambda}\left[V(s)+\frac{2N}{3}s\beta(1+\beta-s)+\frac{Nl^2}{36}(s-3s^2+2-2\beta)\frac{C^2}{s^3}\right] \\
&\quad +\frac{Nl^2}{72\lambda}[(1-s)(1+2s-\beta)s_{xx}-(1+2\beta-s)s\beta_{xx}], \\
0 &= -\frac{1}{\lambda}\left[V(\beta)+\frac{2N}{3}s\beta(1+s-\beta)+\frac{Nl^2}{36}(-s-\beta+1-3s\beta)\frac{C^2}{s^3}\right] \\
&\quad +\frac{Nl^2}{72\lambda}[-\beta(1+2s-\beta)s_{xx}+(1-\beta)(1+2\beta-s)\beta_{xx}].
\end{aligned} \tag{28}$$

If $C = 0$, the directors are constant and previously discussed patterns [11] are recovered. With $C \neq 0$, both homogeneous solutions (s^*, β^*) of (28) (Fig. 5) and highly oscillatory order parameter structures are obtained (Fig. 6). Again, data for $s(0)$, $\beta(0)$, $s_x(0)$, $\beta_x(0)$ are free parameters in these solution classes, which would have to be experimentally imposed along a plane $(x = 0)$ and then Eqs. (27) and (28) prescribe the structure that emerges for $x \neq 0$. Fig. 5 plots the phase space portrait of the homogeneous solutions. The homogeneous equilibria exist above a C-dependent critical concentration N and are truly biaxial; the terms in (28) proportional to C yield new equilibria depicted in Fig. 5 for fixed C, persistence length l, and variable N. The more complex spatial structures captured by (28) are illustrated in Figs. 6 and 7.

5. Equilibria of the 2D DMG model

The 2D orientation tensor $\tilde{\mathbf{Q}}$ can be written in the form of a single order parameter s and director $\tilde{\mathbf{n}}$,

$$\tilde{\mathbf{Q}} = s(\tilde{\mathbf{n}} \otimes \tilde{\mathbf{n}} - \tfrac{1}{2}\tilde{\mathbf{I}}), \tag{29}$$

where $\tilde{\mathbf{n}} \in R^2$ is a unit eigenvector of $\tilde{\mathbf{Q}}$ and the range of values for s is $[-1, 1]$. We now construct special solutions analogous to those above in Section 4.

5.1. Orientation patterns corresponding to transversely varying order parameter and director field

We posit that the order parameter varies in one spatial direction and time, while the director varies in the transverse direction independent of time:

$$\tilde{\mathbf{Q}} = s(x,t)[\tilde{\mathbf{n}}(y) \otimes \tilde{\mathbf{n}}(y) - \tfrac{1}{2}\tilde{\mathbf{I}}]. \tag{30}$$

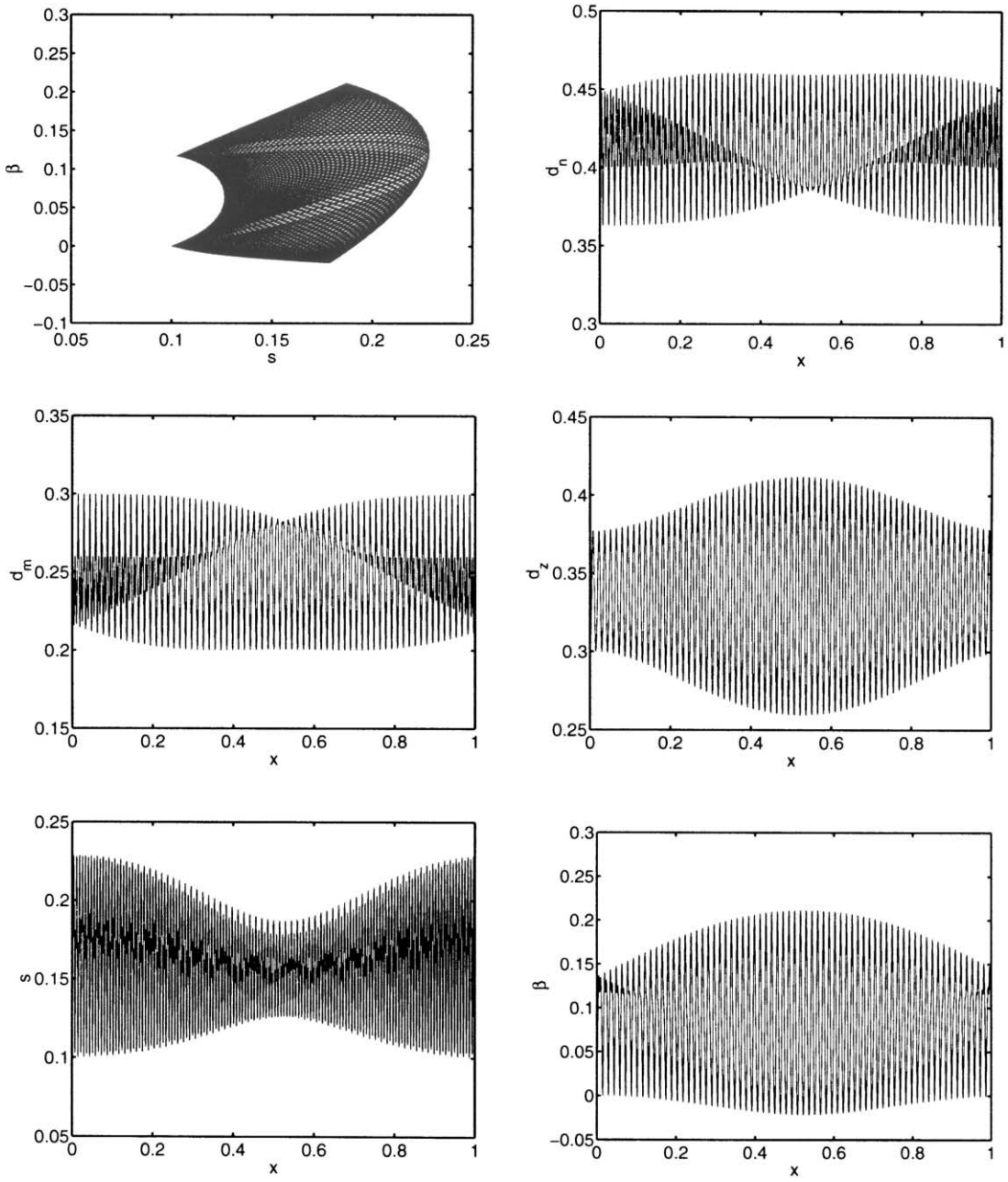

Fig. 6. A spatially nonhomogeneous order parameter solution of (28) corresponding to $C = 5$, $l = 0.01$, $N = 15$. Here we are graphing the order parameters (i.e. degrees of orientation).

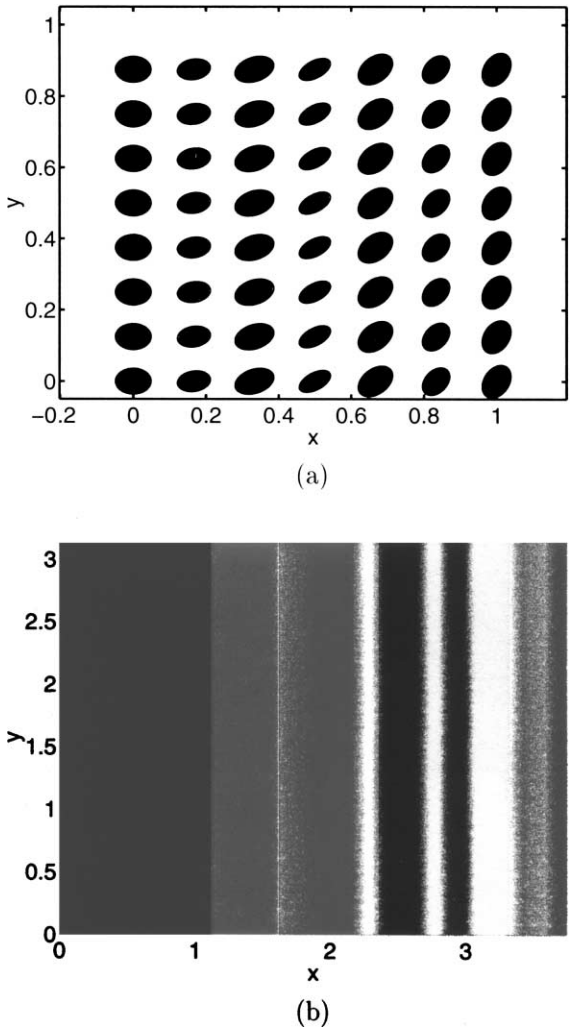

Fig. 7. (a) The spatial orientation pattern of Fig. 6. (b) The light intensity pattern constructed from the orientation pattern of (a) where the intensity is given by the formula in Fig. 3 caption.

In order to attain a self-consistent, closed equation for the order parameter s, we assign $\mathbf{n}$ to be a solution of the second order harmonic equation

$$\frac{\mathrm{d}^2}{\mathrm{d}y^2}\tilde{\mathbf{n}} = -\gamma^2\tilde{\mathbf{n}}, \tag{31}$$

subject to the constraint

$$\frac{\mathrm{d}\tilde{\mathbf{n}}}{\mathrm{d}y} \otimes \frac{\mathrm{d}\tilde{\mathbf{n}}}{\mathrm{d}y} = \gamma^2\tilde{\mathbf{n}}^\perp \otimes \tilde{\mathbf{n}}^\perp, \tag{32}$$

where $\tilde{\mathbf{n}}^\perp$ is the other unit eigenvector of $\tilde{\mathbf{Q}}$ orthogonal to $\tilde{\mathbf{n}}$, and γ an arbitrary constant that will be seen to couple

to the governing equation for s. The general solution of (31) subject to (32) is

$$\tilde{\mathbf{n}} = \begin{pmatrix} \sin(\gamma y + \theta_0) \\ \cos(\gamma y + \theta_0) \end{pmatrix}, \tag{33}$$

with θ_0 an arbitrary constant. With this $\tilde{\mathbf{n}}$, the orientation tensor equation (7) reduces to the scalar reaction–diffusion equation

$$s_t = -\frac{\sigma}{\lambda}\left[U(s) - \frac{Nl^2}{48}(1-s^2)s_{xx}\right], \tag{34}$$

where

$$U(s) = s(1 - \tfrac{1}{2}N + \tfrac{1}{2}Ns^2) + \tfrac{1}{12}Nl^2\gamma^2 s(1-s^2). \tag{35}$$

In steady state,

$$s_{xx} = \frac{48}{Nl^2}\frac{U(s)}{1-s^2}, \tag{36}$$

a Hamiltonian system with Hamiltonian H,

$$H = \frac{(s_x)^2}{2} - \int \frac{48}{Nl^2}\frac{U(s)}{1-s^2}\,\mathrm{d}s = \frac{(s_x)^2}{2} + \frac{12}{l^2}\left(1 - \frac{l^2\gamma^2}{6}\right)s^2 + \frac{24}{Nl^2}\ln|1-s^2|. \tag{37}$$

There are three critical points of (36), Fig. 8, corresponding to the three roots of $U(s)$:

$$s_0 = 0, \qquad s_\pm = \pm\sqrt{1 - \frac{2}{N(1-\frac{1}{6}l^2\gamma^2)}}. \tag{38}$$

The pair $s_\pm$ is real and $|s_\pm| < 1$ only for $\frac{1}{6}l^2\gamma^2 \le 1 - 2/N$, or $N \ge 2/(1-\frac{1}{6}l^2\gamma^2)$. Stability within the reduced ODE (36) is straightforward and typical of pitchfork bifurcations.

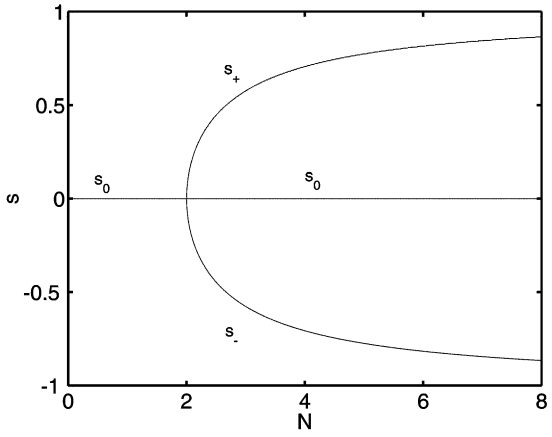

Fig. 8. The 2D order parameter equilibria (38) for $\tilde{\mathbf{Q}}$. The pitchfork bifurcation takes place at $N = 2(1-\frac{1}{6}l^2\gamma^2)^{-1}$. In this figure $l = 0.01,\ \gamma = 10$.

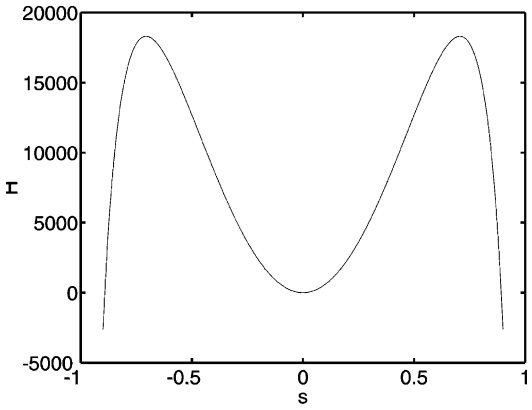

Fig. 9. The potential energy diagram of (37) where $\gamma = 10,\ l = 0.01,\ N = 4$.

The constant anisotropic order parameter solutions $s_{\pm}$, (38), together with the oscillatory director (33), give the 2D DMG theory pattern analogous to the 3D patterns of Section 4.1. Oscillatory steady solutions of (36), again with the periodic director (33), provide the 2D analog of the 3D patterns of Section 4.2. The potential energy diagram of (37) is given in Fig. 9 for $\gamma = l = 1,\ N = 4$. Clearly, there are periodic solutions that oscillate about the isotropic equilibrium $s = 0$ and remain bounded within the physical constraints $s \in [-1, 1]$.

In Fig. 10, we depict the 2D orientation structure captured by oscillatory steady solutions of (36). The optical axis (director) "tumbles" periodically in the y-direction, and is constant in x. The degree of orientation (order parameter) is constant in y, but oscillates periodically in x about the isotropic value $s_0 = 0$. These two pieces of information are conveyed in Fig. 10 by ellipses at each location; the axes are determined by the directors $\tilde{\mathbf{n}}$, $\tilde{\mathbf{n}}^{\perp}$ and the axis lengths are $d_1 = \frac{1}{3}(1 + 2s),\ d_2 = \frac{1}{3}(1 - s)$.

5.2. *Patterns corresponding to unidirectional variation of the order parameter and the director field*

Analogous to the 3D solutions (24) of Section 4.2, we posit

$$\tilde{\mathbf{Q}} = s(x,t)(\tilde{\mathbf{n}}(x,t) \otimes \tilde{\mathbf{n}}(x,t) - \tfrac{1}{2}\tilde{\mathbf{I}}), \tag{39}$$

where

$$\tilde{\mathbf{n}}^{\mathrm{T}} = (\cos\xi(x,t),\ \sin\xi(x,t)). \tag{40}$$

The 2D DMG tensor equation (7) reduces to

$$s_t = -\frac{1}{\lambda}\left[U_0(s) + \frac{Nl^2}{12}s(1-s^2)(\xi_x)^2\right] + \frac{Nl^2}{48\lambda}(1-s^2)s_{xx}, \qquad \xi_t = \frac{Nl^2(s^2\xi_x)_x}{2\lambda s^2}, \tag{41}$$

where

$$U_0(s) = s(1 - \tfrac{1}{2}N(1-s^2)). \tag{42}$$

In steady state, the director angle simplifies as before,

$$s^2\xi_x = C = \text{constant}, \tag{43}$$

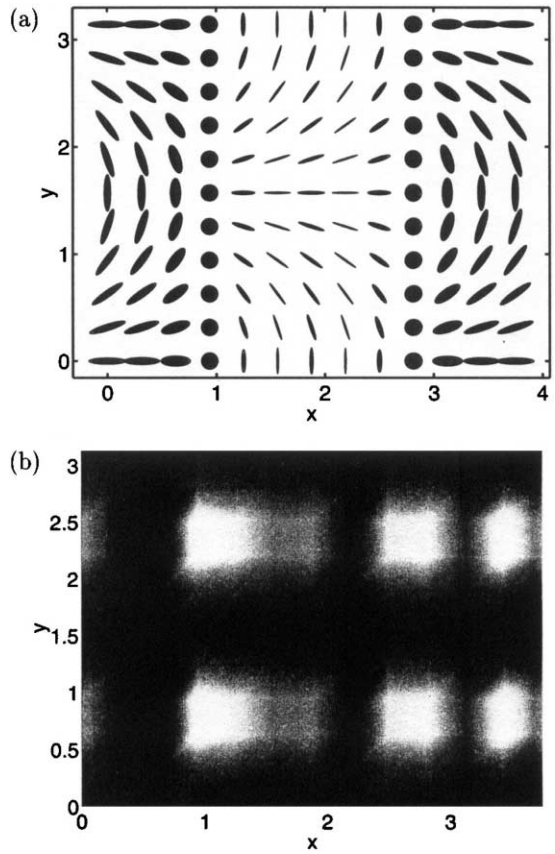

Fig. 10. (a) A spatial orientation pattern of the 2D DMG theory, (33) and (36), where $\gamma = 1$, $l = 1$, $N = 4$, $\theta_0 = 0$. The elliptical semi-axes lengths depict the relative degrees of orientation with respect to the principal axes, which are the director axes. This pattern is distinguished by x-periodic variation of the order parameter (i.e., the ellipse shape deforms along the x-direction) and y-periodic variation of the optical axis (i.e. the director "tumbles" along the y-direction). (b) The light intensity pattern for (a) where the intensity is given by the formula in Fig. 3 caption.

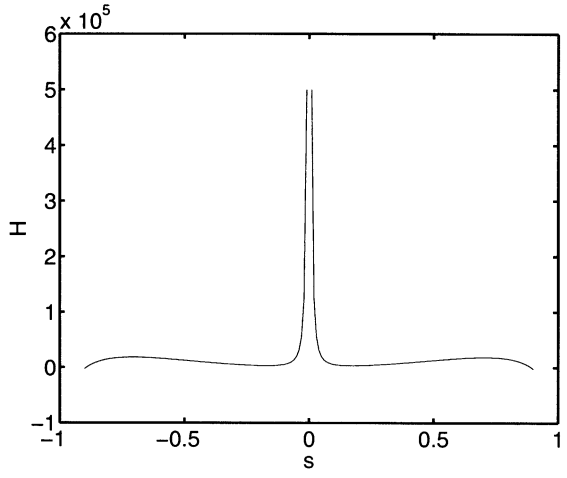

Fig. 11. A diagram of the potential energy (45) where $C = 10$, $l = 0.01$, $N = 4$.

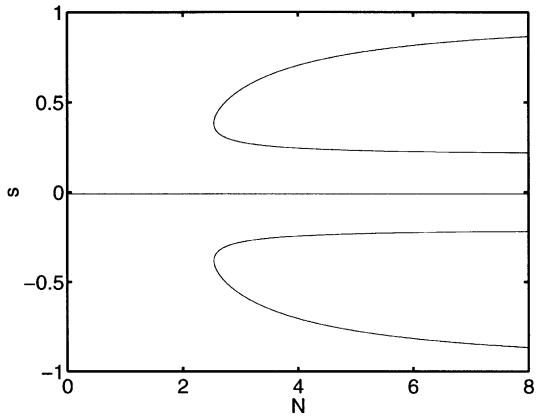

Fig. 12. The behavior of the equilibria (47) as function of N for $l = 0.01,\ C = 10$.

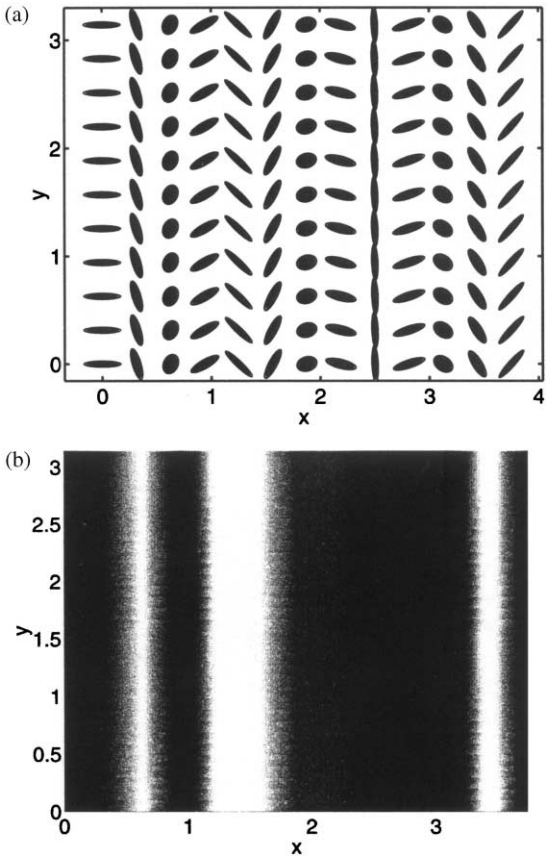

Fig. 13. (a) The spatial pattern of the steady-state solution of (46), where $C = 10,\ l = 0.01,\ N = 4,\ \theta_0 = 0$. (b) The light intensity pattern constructed from the orientation pattern of (a). The intensity is given by $I = I_0 \sin^2(2\pi aB)$, where $B,\ a$ are defined in Fig. 3.

from which we can decouple a scalar nonlinear oscillator equation for s:

$$-\frac{1}{\lambda}\left[U_0(s)+\frac{Nl^2}{12s^3}(1-s^2)C^2\right]+\frac{Nl^2}{48\lambda}(1-s^2)s_{xx}=0. \tag{44}$$

Again, this is a Hamiltonian system with Hamiltonian

$$H=\frac{s_x^2}{2}+\frac{24}{Nl^2}\ln|1-s^2|+\frac{12s^2}{l^2}+\frac{C^2}{2s^2}. \tag{45}$$

Fig. 11 depicts the potential energy (45) for $C=10$, $l=0.01$ and $N=4$.

There are three basic 2D structures captured by this system of equations, analogous to the 3D structures described in Section 4. For $C=0$, the director is constant, and (41) reduces to a scalar reaction–diffusion equation for the order parameter s,

$$s_t=-\frac{1}{\lambda}U_0(s)+\frac{Nl^2}{48\lambda}(1-s^2)s_{xx}. \tag{46}$$

This is a 2D analog of the reaction–diffusion system and patterns derived in [11].

For $C\neq 0$ and s^* a fixed point of (44), we deduce periodic director variation with a homogeneous order parameter. The equilibrium branches $s^*(N,l,C)$ are solutions of

$$s^3U_0(s)+\frac{Nl^2}{12}C^2(1-s^2)=0, \tag{47}$$

which is a cubic equation in s^2. Fig. 12 gives the equilibria of (47) as a function of N for $l=0.01$ and $C=10$.

For $C\neq 0$, and $s(x)$ a periodic solution of (44), we construct a unidirectional 2D pattern whose director tumbles in the x-direction (since the director angle $\xi(x)$ is a monotone function) while the degree of orientation ($s(x)$) oscillates (see Fig. 13).

6. Concluding remarks

A variety of mesoscopic orientation patterns have been constructed from the 3D and 2D Doi–Marrucci–Greco theory without flow, which is the tensorial PDE (7) with $\mathbf{D}=\mathbf{\Omega}=\mathbf{0}$. These exact constructions are developed from a spectral representation of the orientation tensor $\mathbf{Q}$ (3D) or $\tilde{\mathbf{Q}}$ (2D). Remarkably, the tensorial PDE allows one to posit separate $\mathbf{x},t$ dependence of the eigenvalues (order parameters) and eigenvectors (optical axes or directors). Thus, our construction is akin to a geometrical separation of variables in spectral coordinates of $\mathbf{Q}$. The result is a wide class of exact mesoscale patterns which exist purely between short-range excluded-volume and intermediate-range distortional elasticity potentials. These exact solutions are useful as guides in full flow–nematic simulations, and even as nontrivial benchmarks for numerical codes. Indeed, from our own mathematical perspective, classes of exact solutions help to de-mystify otherwise imposing tensorial PDEs.

We have shown on one hand that no direct correspondence exists between a formal 2D $\tilde{\mathbf{Q}}$ theory and the standard 3D $\mathbf{Q}$ theory. On the other hand, the "planar" and "unidirectional" structures that we have derived from the 3D DMG theory are shown to have close analogs in the 2D $\tilde{\mathbf{Q}}$ theory. Thus, the 2D theory has qualitative value even though no direct physical information is captured.

We emphasize these exact solutions, which we have then used to infer exact light scattering intensity patterns, are mathematical models for the flow-induced structures widely reported among experimentalists [4,6,7,14,15]. The

fate or role of these structures in flows will be tenuous at best, since any imposed or interacting flow necessarily alters the equations we have derived these solutions from. The mathematics of the flow–nematic interactions, Eqs. (7)–(10), is significantly more complex. Witness the rich bifurcation theory that underlies the phase diagram for simple imposed flows and only an excluded-volume nematic potential [10,11]. Rigorous mathematics beyond what we have indicated here requires brain power, creativity, and zeal as displayed for many years by Prof. Zakharov.

Acknowledgements

Effort sponsored by the Air Force Office of Scientific Research, Air Force Materials Command, USAF, under Grant Nos. F49620-97-1-0001 and F49620-99-1-0003. The US Government is authorized to reproduce and distribute reprints for governmental purposes notwithstanding any copyright notation thereon. The views and conclusions contained herein are those of the authors and should not be interpreted as necessarily representing the official policies or endorsements, either expressed or implied, of the Air Force Office of Scientific Research or the US Government.

References

[1] A.V. Bhave, Kinetic theory for dilute and concentrated polymer solutions: study of nonhomogeneous effects, Ph.D. Thesis, Massachusetts Institute of Technology, 1992.
[2] A.N. Beris, B.J. Edwards, Thermodynamics of Flowing Systems with Internal Microstructure, Oxford Science Publications, Oxford, 1994.
[3] B. Bird, R.C. Armstrong, O. Hassager, Dynamics of Polymeric Liquids, Vols. 1 and 2, Wiley, New York, 1987.
[4] W.R. Burghardt, Molecular orientation and rheology in sheared lyotropic liquid crystalline polymers, Macromol. Chem. Phys. 199 (1998) 471–488.
[5] M. Doi, Molecular dynamics and rheological properties of concentrated solutions of rod-like polymers in isotropic and liquid crystalline phases, J. Polym. Sci. 19 (1981) 229–243.
[6] M. Doi, S.F. Edwards, The Theory of Polymer Dynamics, Oxford University Press/Clarendon Press, London/New York, 1986.
[7] A.M. Donald, A.H. Windle, Liquid Crystalline Polymers, Cambridge University Press, 1992.
[8] J. Feng, L.G. Leal, Pressure-driven channel flows of a model liquid-crystalline polymer, Phys. Fluids 11 (1999) 2821–2835.
[9] J. Feng, L.G. Leal, Simulating complex flows of liquid crystalline polymers using the Doi theory, J. Rheol. 41 (1997) 1317–1335.
[10] M.G. Forest, Q. Wang, H. Zhou, Homogeneous biaxial patterns and director instabilities of liquid crystal polymers in axial and planar elongation, Phys. Fluids 12 (3) (2000) 490–498.
[11] M.G. Forest, Q. Wang, H. Zhou, Exact banded patterns from a Doi–Marrucci–Greco model of nematic liquid crystal polymers, Phys. Rev. E 61 (6) (2000) 6655–6662.
[12] M.N. Kawaguchi, M.M. Denn, A mesoscopic theory of liquid crystalline polymers, J. Rheol. 43 (1) (1999) 111–124.
[13] R. Kupferman, M.N. Kawaguchi, M.M. Denn, Emergence of structure in models of liquid crystalline polymers with elastic coupling, Preprint, 1999.
[14] R.G. Larson, Constitutive Equations for Polymer Melts and Solutions, Butterworths, London, 1988.
[15] R.G. Larson, The Structure and Rheology of Complex Fluids, Oxford University Press, Oxford, 1999.
[16] P.L. Maffettone, S. Crescitelli, Bifurcation analysis of a molecular model for nematic polymers in shear flows, J. Non-Newtonian Fluid Mech. 59 (1995) 73–91.
[17] W. Maier, A. Saupe, Eine einfache molekulare theorie des nematischen kristallinflussigen zustandes, Z. Naturforsch. A 13 (1958) 564–566.
[18] G. Marrucci, F. Greco, The elastic constants of Maier–Saupe rod-like molecule nematics, Mol. Cryst. 206 (1991) 17–30.
[19] P.T. Mather, A. Romo-Uribe, C.D. Han, S.S. Kim, Rheo-optical evidence of a flow-induced isotropic–nematic transition in a thermotropic liquid crystalline polymer, Macromolecules 30 (25) (1997) 7977–7989.
[20] L. Onsager, The effects of shape on the interaction of colloidal particles, Ann. NY Acad. Sci. 51 (1949) 627–659.
[21] V.M. Pergamenshchik, Spontaneous deformations of the uniform director ground state induced by the surface-like elastic terms in a thin planar nematic layer, Phys. Rev. E, in press.

[22] T. Tsuji, A. Rey, Orientation mode selection mechanisms for sheared nematic liquid crystalline materials, Phys. Rev. E 57 (5) (1998) 5609–5625.
[23] V.E. Zakharov, Kolmogorov spectra in weak turbulence problems, Handbook Plasma Phys. 2 (1984) 1–36.
[24] V.E. Zakharov, V. Lvov, G. Falkovich, Kolmogorov Spectra of Turbulence I, Springer, New York, 1992.
[25] V.E. Zakharov, A.B. Shabat, Exact theory of two-dimensional self-focusing and one-dimensional self-modulation of waves in nonlinear media, Sov. Phys. JETP 34 (1972) 62–69.